Transactions of the Materials Research Society of Japan 29 [2] 603-606 (2004)

Effects of Ion Microbeam Irradiation on Silica Glass

H. Nishikawa, K. Fukagawa, T. Yanagi*, Y. Ohki*, E. Watanabe**,
M. Oikawa***, T. Kamiya***, and K. Arakawa***
Shibaura Inst. Tech., 3-9-14 Shibaura, Minato-ku, Tokyo 108-8548, Japan
Fax:81-3-5476-3068, e-mail:nishi@sic.shibaura-it.ac.jp
*Waseda Univ., 3-4-1 Ohkubo, Shinjuku-ku, Tokyo 169-8555, Japan
Fax: 81-3-3204-1258, e-mail:yohki@waseda.jp
**Tokyo Metropolitan Univ., 1-1 Minami-Osawa, Hachioji, Tokyo 192-0397, Japan
Fax: 81-427-77-2756, e-mail:eiki@eei.metro-u.ac.jp
***Japan Atomic Energy Research Inst., 1233 Watanuki-machi, Takasaki-shi, Gunma, 370-1292, Japan
Fax:81-27-346-9690, e-mail:kazuo@taka.jaeri.go.jp

Silica glasses were implanted with H^+ or Si^{5+} at the microbeam facility of TIARA (JAERI Takasaki, Japan). Micron and sub-micron scale radiation effects induced by ion microbeam were studied using a confocal optical microscope equipped with a monochromator under excitation with an Ar ion laser. Three dimensional mappings of Raman scattering and photoluminescence (PL) features of the microbeam irradiated area in silica glass indicate the formations of the luminescent dangling bonds and small ring structures associated with the compaction of silica glass. Surface topology was also investigated by an atomic force microscope, showing the formation of surface grooves due to the internal compaction of silica glass. Technological implications of these results on the possible application of the ion microbeam techniques to the fabrication of optical elements will be discussed.
Key words: ion microbeam, silica, optical elements, Raman scattering, photoluminescence

1. INTRODUCTION

Owing to the high transparency and durability, silica glass is one of the most promising optical materials for the substrates of various applications using ion-beam processing techniques. Effects of ion implantation on silica glass include structural compaction and resulting refractive index changes up to an order of 10^{-2}, which has been used for fabrication of various optical elements such as long-period optical fiber gratings[1]. We have studied this phenomenon using an ion microbeam technique for fabrication of micrometer-scale optical elements on silica glass[2,3].

Rapid growth of the data traffic on the internet drives the development of wavelength division multiplexing (WDM) technique. Optical filters using fiber Bragg gratings (FBG) is one of the most important optical elements for the WDM. Writing with ion beam is advantageous over a conventional UV writing technique of the FBG[4], since no special pre-treatment of silica glass is involved for enhanced photosensitivity. Also, a better stability of induced grating structure is assured by ion implantation.

In this study, we report the results of radiation effects induced by ion microbeam irradiation on silica glass. Application of the ion microbeam to direct writing of grating on waveguide is also discussed.

2. EXPERIMENTAL PROCEDURES

Samples are high-purity silica ([OH]; 1200 ppm) with a dimension of $3\times3\times10$ mm^3. The samples were irradiated either by H^+ microbeam through a 4-μm thick mylar film for vacuum retention membrane using a 3-MV single-ended accelerator, or by Si^{5+} microbeam under vacuum using a 3-MV tandem accelerator (TIARA, JAERI Takasaki).

The ion microbeam focused to a diameter of ~1 μm was line-scanned over a sample edge region perpendicular to an edge line with a length of ~50 μm, and widths varied from 10 to 40 μm. Radiation effects induced by ion microbeam were investigated by means of micro-Raman/photoluminescence (μ-Raman/PL) spectroscopy, an atomic force microscopy (AFM), and optical microscopy. Lateral and axial spatial resolutions are respectively estimated to be 4 μm and 20 μm for Raman scattering (JASCO, NRS2100) and 1 μm and 0.8 μm for PL (Tokyo Instruments, Nanofinder) measurements.

In addition, a microscopic two-beam interferometer was used to evaluate refractive index changes in microbeam irradiated regions in silica glass.

3. RESULTS AND DISCUSSION

3.1 Phase microscope images

Figure 1 shows a phase microscope image obtained from the side surface of silica glass on which the H^+-microbeam was scanned at different widths. At the stopping range of H^+, the lateral spread of refractive index changed region represented as a bright area in Fig. 1, is estimated to be 8 μm for the microbeam-scanned width of 1 μm (see the rightmost rectangular region). The lateral straggling for H^+ ion distribution is estimated to be ~1.6 μm by a TRIM simulation. Since a significant stress buildup is expected at the site of the compaction in the projected range, the compacted region can induce further structural relaxation and refractive index change

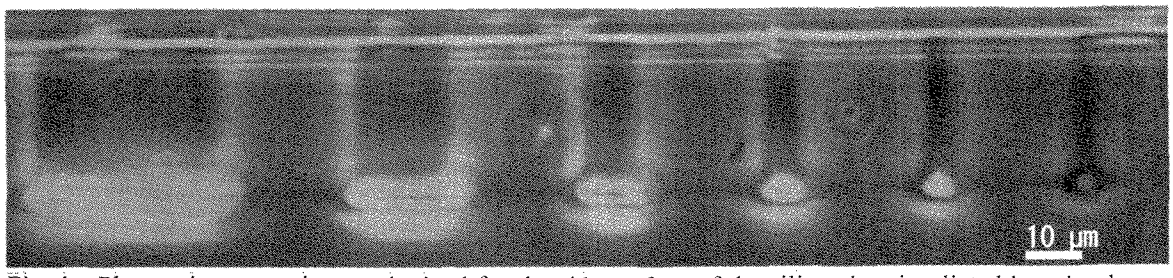

Fig. 1 Phase microscope image obtained for the side surface of the silica glass irradiated by microbeam (H^+, energy: 1.7 MeV, fluence: 1×10^{17} ions/cm^2) with different irradiation widths of 40, 20, 10, 5, 3, and 1 μm from left to right.

in the surrounding SiO_2 network. Therefore, the broader lateral distribution width of 8 μm at the projected range corresponds to distribution of the structural relaxation of silica glass.

On the other hand, although the refractive index change is not so significant, the lateral spread near the irradiation surface is smaller, when compared with the stopping range.

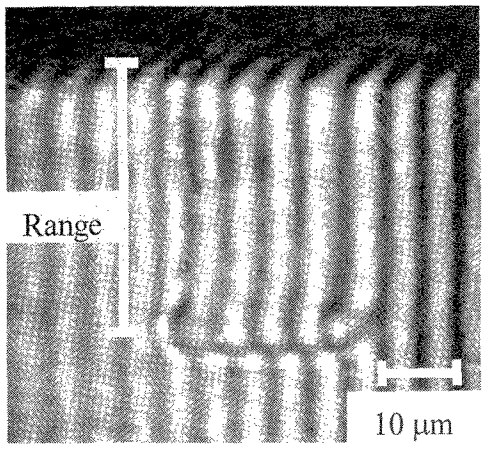

Fig. 2 Interference fringes taken by a microscopic two-beam interferometer, obtained for H^+ microbeam irradiated region (1.7 MeV, 1×10^{17} cm^{-2}, width: 20 μm).

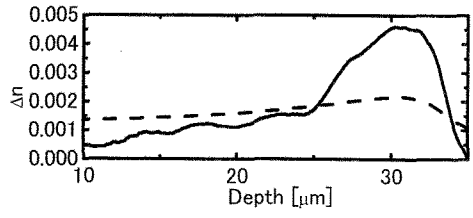

Fig. 3 Refractive index change (Δn) measured by a microscopic two-beam interferometer (solid line) from Fig. 2 and that estimated by an atomic force microscope (broken line) for (1.7 MeV, 1×10^{17} cm^{-2}, width: 20 μm).

3.2 Depth profile of refractive index change

Figure 2 shows an image obtained by a microscopic two-beam interferometer for the H^+-beam-scanned area with 20 μm width. At the stopping range of ions, large displacements of the interference fringes were observed. Since the displacement of the fringe is proportional to refractive index change Δn, it is possible to estimate Δn as a function of the depth from the surface.

Figure 3 shows the depth distribution of Δn (solid line) estimated from the interference fringes in Fig. 2. Also shown is Δn (broken line) obtained from the compaction of silica glass, which is calculated from the surface grooves measured at the side and front surfaces by AFM measurements using the Lorentz-Lorenz relationship [5].

$$\Delta n = -\frac{(n^2-1)(n^2+2)}{6n}\cdot\frac{\Delta V}{V} \qquad (1)$$

The result from the microscopic two-beam interferometer shows the maximum of the H^+-microbeam-induced Δn at the depth of 32 μm. This is in fair agreement with the result of Δn estimated by AFM. Relatively large discrepancy at the projected range may be due to errors in estimating the internal compaction of silica glass from the depth of the grooves at the front and side surfaces by the AFM measurement. We also note that Δn with an order of magnitude of lower value is induced at the track of ions than the stopping range.

3.3 Raman scattering

Figure 4 shows μ-Raman spectra at the 40 μm-width microbeam-scanned area measured at different depths from the irradiation surface. At the stopping range (32 μm) of H^+, a significant increase was observed for the Raman scattering intensity at 606 cm^{-1} due to three-membered rings[6], which are smaller than regular ring sizes of five- or six-membered rings in silica glass networks. This supports the mechanism of

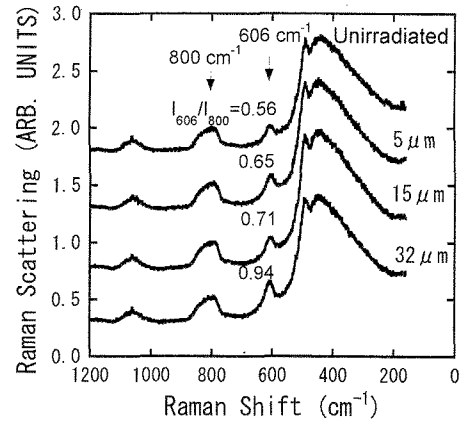

Fig. 4 μ-Raman spectra obtained for the irradiation width of 40 μm at different depths from the surface (H^+, 1.7 MeV, fluence: 1×10^{17} cm^{-2}). The 606 cm^{-1} intensity is shown as an intensity ratio to the 800 cm^{-1} peak due to Si-O-Si bending mode.

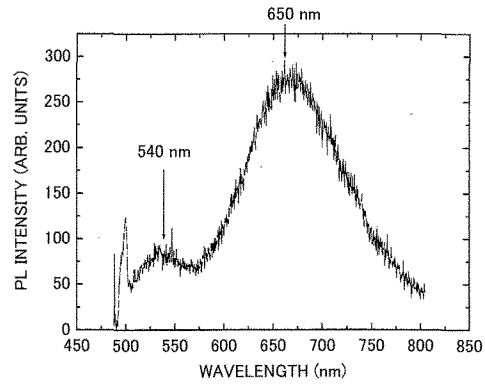

(a) PL spectrum

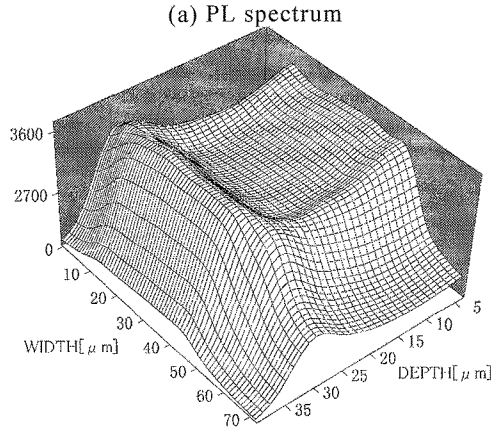

(b) Distribution of the 650 nm band

Fig.5 (a)PL spectra and (b)two-dimensional PL intensity distributions of the 650 nm band obtained for the irradiated region with a line width of 40 μm (H^+, energy: 1.7 MeV, fluence:1×10^{17} cm^{-2}).

refractive index changes according to Eq. (1) due to the compaction of silica glass induced by ion beam irradiation.

3.4 Photoluminescence

To obtain more insight into the effects of microbeam irradiation on the structure of silica glass, μ-PL measurements were performed. Fig. 5 (a) shows PL spectra at room temperature under excitation at 488 nm. Two PL bands at 540 nm and 650 nm are observed at the surface of the microbeam irradiated regions. The PL band at 650 nm is due to nonbridging oxygen hole centers[7] (NBOHCs, ≡Si-O・, where the symbols "≡" and "・", respectively, represent separate three bonds with three oxygens and an unpaired electron), while the origin of the 540 nm band was not previously reported.

The depth profile of the PL intensity at 650 nm was performed on the sample from the side surface. Fig. 5 (b) shows a PL mapping image obtained for the side surface of the sample. The distribution of the PL intensity due to NBOHCs can be seen from the surface along the tracks of ions with a maximum at the range.

3.5 Mechanisms of defect generation and compaction

Figure 6 shows a result obtained by a TRIM98 simulation [8] for silica irradiated with a 4-μm-thick mylar film on the surface implanted with H^+ ions at 1.7 MeV. The energy deposition by electronic stopping power is dominating over the entire track of ions, while the energy deposited by nuclear stopping power is less than 1% of total deposited energy.

Since the profile of the electronic stopping power in Fig. 6 is similar to that observed PL in Fig.5 (b), the electronic stopping power is responsible for the defect generation. The formation mechanism of the NBOHC is due to the breaking of normal Si-O bond:

$$\equiv Si\text{-}O\text{-}Si \rightarrow Si\text{-}O\cdot + \cdot Si\equiv, \qquad (2)$$

which is driven by the non-radiative decay of self-trapped excitons produced under dense excitations along the tracks of ions[9]. The formation reaction of equation (2) is consistent with our previous ESR study on H^+ irradiated silica glass, where the pair creation of NBOHC and its counterpart, the E' center (≡Si・) was observed [10].

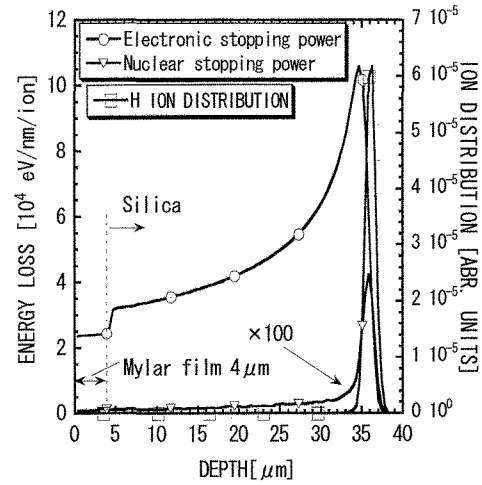

Fig. 6 Energy deposition and ion distribution calculated by TRIM 98 simulation for silica with a 4-μm-thick mylar film on the surface implanted with H^+ ions at 1.7 MeV.

The refractive index change profile shown in Fig.3 is also in good agreement with that of energy deposition by electronic stopping power from the surface to the projected range. Taking into account the increased small-ring structures such as three-membered rings from Raman spectra in Fig. 4, the refractive index change due to compaction of silica glass is determined by the electronic stopping power. However, at the projected range of ions, we cannot rule out the effect of nuclear stopping [11] as well as electronic one on the refractive index change.

3.6 Application for writing gratings

Periodic modulation of refractive index at intervals as small as 0.5 μm at the core of a waveguide is required to fabricate the Bragg gratings [4], which can selectively reflect a specific wavelength of light in the WDM system for optical communication at 1.55 μm. Therefore, the lateral spread of the refractive index changes should be minimized for the direct

writing of the Bragg gratings using ion microbeam, while a sufficient Δn of 10^{-3} order is achieved as shown in Fig.3. A possibility for the better resolution in direct writing by H^+ microbeam may be achieved by the use of radiation effect near the surface rather than that at the stopping range, though an order of higher fluence is required.

Figures 7 (a) and (b) show optical microscope images obtained for the cross sections of the samples irradiated by the microbeam of H^+ and Si^{5+}, respectively. Refractive index changes can be seen as white bright regions by the transmitted light through samples illuminated from the other surface. For the case of H^+ irradiation, the fluence of 10^{17} cm^{-2} order is required to observe the refractive index change at the track of ions, while 10^{14} cm^{-2} is enough for Si^{5+}. This is due to the fact that energy deposition per unit length is about two orders of magnitude lower for H^+ than for Si^{5+}.

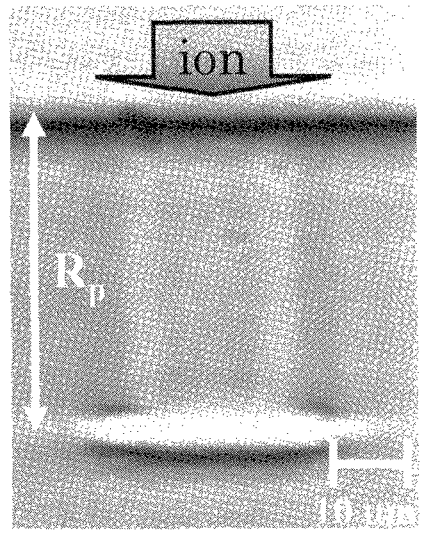

(a) H^+

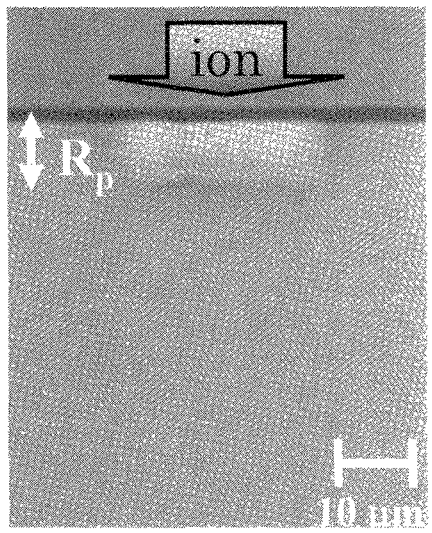

(b) Si^{5+}

Fig. 7 Optical microscope images obtained for samples irradiated by the microbeams of (a) H^+ (1.7 MeV, fluence:1×10^{17} cm^{-2}, width: 20 μm) and (b) Si^{5+} (18 MeV, fluence: 1×10^{14} cm^{-2}, width: 20 μm). The R_p represents a projected range.

Figure 7 (a) shows that the refractive index change is inhomogeneous over the entire track of ions for H^+ microbeam. Figure 7 (a) shows that the induced refractive index change is highest at the projected range by the 1.7-MeV H^+ microbeam. Therefore, H^+ microbeam is appropriate to induce a localized refractive index change at buried optical channel, such as the core of optical fibers, as previously reported for writing of long-period gratings [1]. On the other hand, the refractive index change by Si^{5+} microbeam is localized at the surface with smaller lateral spread, as shown in Fig. 7 (b). This suggests a possibility of the heavy-ion microbeam for the writing of gratings on the surface of planar optical waveguides.

4. SUMMARY

Effects of H^+ or Si^{5+} microbeam irradiation on silica glasses were investigated by an optical microscope, AFM, μ-Raman, and μ-PL measurements.

The refractive index change in the micrometer-sized area scanned by ion microbeam is explained by internal compaction of silica glasses. Energy deposition by electronic stopping power is responsible for the compaction accompanied by the breaking of Si-O bonds.

Since the spatial distribution of radiation effects such as the compaction and resulting refractive index changes greatly differ between the 1.7 MeV H^+ and 18 MeV Si^{5+}, proper choice of ion species is important to apply the ion microbeam to the direct writing of grating devices, depending on the forms of target waveguides such as optical fibers and planar circuits.

References

[1] M. Fujimaki, Y. Nishihara, Y. Ohki, J. L. Brebner, and S. Roorda, J. Appl. Phys. 88, 5534 -5537 (2000)
[2] M. Hattori, Y. Ohki, M. Fujimaki, T. Souno, H. Nishikawa, E. Watanabe, M. Oikawa, T. Kamiya, and K. Arakawa, Nucl. Instr. and Meth. in Phys. Res. B 210, 272-276 (2003)
[3] T. Souno, H. Nishikawa, M. Hattori, Y. Ohki, M. Fujimaki, E. Watanabe, M. Oikawa, T. Kamiya, and K. Arakawa, Nucl. Instr. and Meth. in Phys. Res. B 210, 277-280 (2003)
[4] K. O. Hill, Y. Fujii, D. C. Johnson, and B. S. Kawasaki, Appl. Phys. Lett. 32, 647-649 (1978)
[5] B. Poumellec, P. Niay, M. Douay, and J. F. Bayon, J. Phys. D: Appl. Phys. 29, 1842-1856 (1996)
[6] F. L. Galeener, J. Non-Cryst. Solids, 71, 373-386 (1985)
[7] L. Skuja, J. Non-Cryst. Solids 179, 51 (1994)
[8] "The Stopping and Range of Ions in Solids", by J. F. Ziegler, J. P. Biersack and U. Littmark, Pergamon Press, New York (1985)
[9] N. Matsunami and H. Hosono, Phys. Rev. B60, 10616-10619 (1999)
[10] M. Hattori, Y. Nishihara, Y. Ohki, M. Fujimaki, T. Souno, H. Nishikawa, T. Yamaguchi, E. Watanabe, M. Oikawa, T. Kamiya, and K. Arakawa, Nucl. Instr. and Meth. in Phys. Res. B 191, 362-365 (2002)
[11] R. A. B. Devine, Nucl. Instr. and Meth. in Phys. Res. B 91, 378-390 (1994)

(Received October 9, 2003; Accepted January 20, 2004)